International Journal of Engineering Research & Technology (IJERT)
ISSN: 2278-0181
Vol. 6 Issue 04, April-2017

Space-Vector based Advanced Pulse Width Modulation Techniques for Z-Source Inverter

Mr. Kanan Kumar Das
Lecturer,
Department of Electrical Engineering,
Templecity Institute of Technology and Engineering (TITE),
Bhubaneswar, India

***Abstract*— The Performances of an inverter depends on what type of modulation strategies is used to switch. There exists different types of classical and advanced Pulse Width Modulation (PWM) techniques to switch the traditional Voltage Source Inverter (VSI).The advanced PWM techniques are superior to classical PWM techniques in respect of load current ripple, Total Harmonic Distortions, switching losses. The same concept of advanced PWM techniques for VSI is applicable for Z-Source Inverter. This paper proposes certain vector sequences based on advanced PWM techniques for ZSI. The proposed vector sequences are analysed in respect of load/line current ripple based on stator flux ripple concept. The superiority of the advanced PWM techniques over classical is verified by simulation study of a ZSI in Power-Sim (PSim9.1.1) for R-L and different motor load conditions.**

Keywords*— Bus-Clamping, Current Ripple, Pulse Width Modulation, Maximum Boost Control, Z-Source Inverter

I. INTRODUCTION

Z-source Inverter (ZSI) or Impedance Source Inverter (ISI) is extensively used in different field of application like motor drives **[1]**, electric vehicles **[2]**, photovoltaic system **[3]**, uninterruptible power supply **[4]** etc**.** The X-shape lattice type impedance network present in between the DC input source and the inverter power circuit, is responsible for the unique buck-boost capability of ZSI. The Z-source concept can be applied to all DC-to-AC, AC-to-DC, AC-to-AC and DC-to-DC power conversion **[5]**. There exists little interest in the control methodologies improvement for ZSI. Space vector based PWM techniques for ZSI finds little interest among the researchers. This paper presents an extensive study on space vector based PWM techniques for ZSI.

In literature, ZSI has been analyzed for different control strategies like Simple Boost Control (SBC) **[5],** Maximum Boost Control (MBC) **[6]** and Constant Boost Control (CBC) **[7]**. The MBC gives the highest boosting factor and lowest voltage stress across the switching devices. The MBC can be implemented in carrier based PWM approach or space vector based PWM approach **[6-10].** Extensive study has already been done for carrier based PWM approach for ZSI **[6-10].** The space vector based PWM approach with MBC came in picture in the year of 2012 **[9].** Further there has a few study of ZSI for Bus-Clamping PWM (BCPWM) technique **[10]**. BCPWM is one of the advanced PWM techniques introduced for VSI. Further, the advanced Bus clamping PWM (ABCPWM) techniques have been introduced. These ABCPWM techniques are sometimes known as "Double Switching PWM" techniques as a phase is double switched over a sub-cycle. As compared to classical Space vector PWM techniques, the BCPWM and ABCPWM techniques perform better in respect of load current ripple, load current distortions and lesser switching losses. These PWM techniques have been already proved superior performances compare to classical space vector PWM for VSI based motor drive application theoretically as well as experimentally [11-14].

In motor drive application, ZSI becomes a popular choice for its unique features. But the lesser harmonic distortion in the line current is desirable features for the drive application. For this reason, this paper introduces certain vector sequences with proper shoot-through period based on advanced PWM techniques. The expressions for line current ripple for different sequences have been derived based on the stator flux ripple concept. For the verification of the superiority of advanced PWM techniques, a model of ZSI has been simulated using standard Power-Sim (PSim9.1.1) for R-L and different motor load conditions.

The organization of this paper is as follows- in section-II, the discussion regarding conventional ZSI. In section-III, the different space vector based advanced PWM techniques for VSI have been presented. In section-IV, the shoot-through state of ZSI is discussed. The space vector based different PWM techniques for ZSI have been proposed in section-V. In section-VI, the Maximum Boost Control for space vector PWM has been presented. In the following section-VII, the theoretical analysis of line current ripple based on stator flux ripple for different proposed vector sequences have been elaborated. The simulation results for R-L load and different motor load conditions for different vector sequences have been presented in section-VIII.

II. CONVENTIONAL Z-SOURCE INVERTER

Conventional Z-Source Inverter (ZSI) was introduced in the year of 2003 by Prof. P.Z. Peng **[5].** The boost capability of ZSI is achieved by the application of shoot-through state which is not possible in VSI or CSI (Current Source Inverter). The power circuit for ZSI is shown in Fig-1. During the shoot-through state, the input diode, D_i is in the reverse biased mode and the inductors L_1 and L_2 get charged by the capacitors C_1 and C_2. This state is achieved by the application of simultaneously turn on the two switches in a leg or simultaneously turn on the four switches of two legs or simultaneously turn on all the switches of three legs. During the active state, the diode will be in conduction mode and the inductors will discharges to the load side and charge the capacitor. On the zero state, the load side is totally disconnected from the impedance network, the inductors

International Journal of Engineering Research & Technology (IJERT)
ISSN: 2278-0181
Vol. 6 Issue 04, April-2017

discharge to the capacitors. By volt-sec balance across the inductors the different relationships between different quantities can be found out. The different quantities for ZSI are tabulated in Table-1. Where D_0 is the shoot-through duty ratio and M is the space vector based modulation index (varies from 0 to 0.866) and V_{in} is the input DC voltage to the ZSI. The boosting factor, *B* is defined as the ratio between the Z-network output voltages, V_b to the input DC voltage, V_{in}. The boosting factor depends on D_0 which further depends on the shoot-through duration and sub-cycle period, T_s. Further, D_0 depends on the modulation index, *M*. For different control strategies, the D_0 is different. The overall gain of the inverter can be controlled by controlling both modulation index and boosting factor.

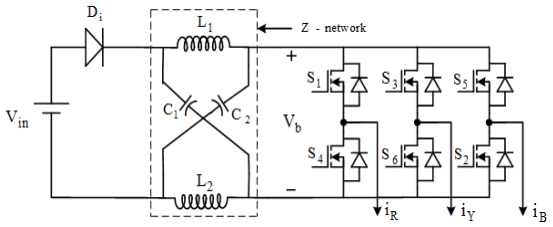

Fig. 1: Power circuit for conventional ZSI

Table-1: Expression for different quantities for Z-source Inverter

Index	Symbol	Expression
Boosting Factor	B	$\frac{1}{1-2D_0}$
Output voltage of Z-network	V_b	$\frac{V_{in}}{1-2D_0}$
Capacitor (C_1) Voltage	V_{C1}	$\frac{1-D_0}{1-2D_0}V_{in}$
Capacitor (C_2) Voltage	V_{C2}	$\frac{1-D_0}{1-2D_0}V_{in}$
Overall Gain	G	$\frac{2}{3}M \times B$
Peak Phase Voltage	$\hat{V}_{ph}$	$\frac{2}{3}M V_b$

III. ADVANCED PWM TECHNIQUES FOR VSI

PWM techniques can be broadly classified into two categories namely carrier based PWM techniques and space vector based PWM techniques. Space vector based PWM techniques give better performances compare to carrier based PWM techniques like better DC bus utilization, lesser Total Harmonic Distortion (THD) and lesser switching losses. Conventional Space Vector PWM (CSVPWM) is one of the most popular and simplest space vector PWM techniques. In space vector approach, each state of the inverter generates a vector of fixed magnitude and angle with reference in space vector plane. For 2-level VSI, there exists eight vectors which can be generated by eight switching state of VSI. Among eight vectors, six are known as active vectors (corresponding switching state is known as active state) and two zero or null vectors (corresponding switching state is known as zero or null state). Active vectors have fixed magnitude and fixed angle with reference whereas the zero or null vectors have zero magnitude. These eight vectors form a hexagon in space vector plane. The null vectors are located at the origin whereas each corners of the hexagon is occupied by the active vector. The hexagon for 2-level VSI is shown in Fig.2(a). The hexagon has six sectors of 60^0 spatial duration each. Each sector is formed by two active vectors and two zero vectors. The reference vector corresponding desired output voltages revolves inside the hexagon at a continuous fashion. To generate the reference vector in continuous fashion, sampling of the reference vector has to be considered inside the hexagon. The reference vector is sampled once in every sub-cycle, T_s. As the positions of the space vectors in hexagon are fixed, the reference vector at any position in a sector can be generated by applying nearby active vectors and zero vectors in such way that the volt-sec balance over a sample period or sub-cycle period can be achieved. The time durations for which the active and zero vectors are applied are known as "dwell times". The dwell times remain same for all the sectors. The expressions for dwell times corresponding active vector-1, active vector -2 and null vector- 0/7 in sector-1 are as follows-

$$T_1 = M\frac{\text{Sin}(60^\circ - \alpha)}{\text{Sin}60^\circ}T_s\,;\,T_2 = M\frac{\text{Sin}\alpha}{\text{Sin}60^\circ}T_s\,;\,T_0 = T_s - T_1 - T_2 \qquad (1)$$

where α is the angle between the reference vector and the starting vector of the sector (active vector-1 in sector-1). The range of α is 0^0 to 60^0. For generating the reference vector, the near-by active vectors and zero vectors need to be applied in a sequence such that the switching losses in the inverter is minimum and the better quality of output waveforms can be achieved. For that the selection of vector sequence in a sample cycle or sub-cycle period, T_s should be satisfy the following conditions-

1. At least one zero vector must be present.
2. Two nearby active vectors must be present.
3. The maximum no of switching must be less than or equal to three.
4. In state transition, only one phase should be switched
5. The dwell times should be divided among vectors in such way that the Volt-Sec balanced can be achieved.

The reference vector in any sector can be generated by applying different vector sequences which are obeyed the above mentioned conditions (1 to 5). The initial vector in the vector sequences can be any vectors among four vectors in sector-1 (0,1,2 and 7). Fig-3 and Table-2 summarises the different valid and not-valid vector sequences possible in sector-1.

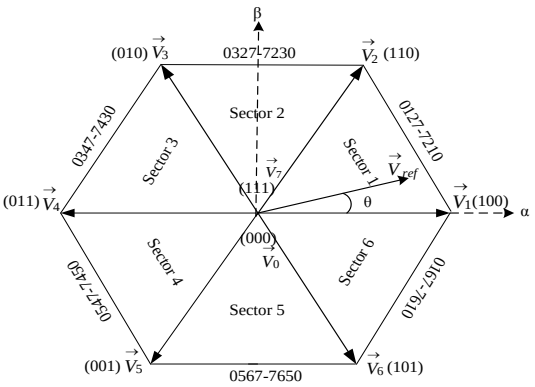

(a)

International Journal of Engineering Research & Technology (IJERT)
ISSN: 2278-0181
Vol. 6 Issue 04, April-2017

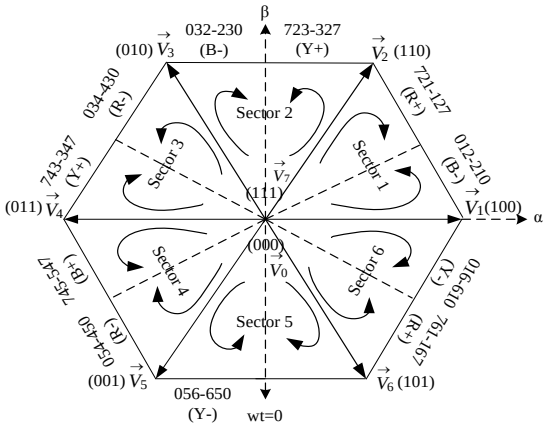

(b)

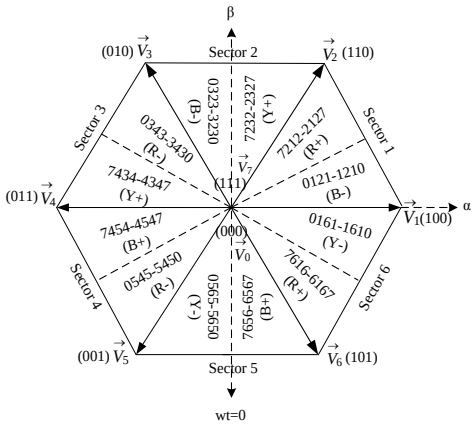

(c)

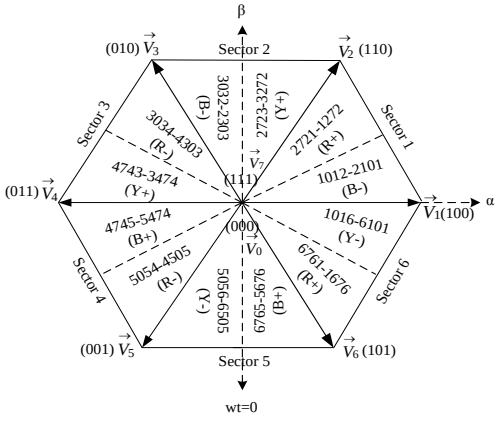

(d)

Fig.2: Space Vector Hexagon for 2-level VSI for (a) CSVPWM (0127-7210), (b)30^0 BCPWM (012-210), (c) Special PWM-1 (0121-1210) and (d) Special PWM-2 (1012-2101)

(0127-7210) vector sequence is popularly known as conventional space vector PWM. (0121-1210) and (7212-2127) vector sequence are known as special PWM type-1 or Advanced Bus-Clamping PWM (ABCPWM) type-1. Whereas vector sequence (1012-2101) and (2721-1272) are named as special PWM type-2 or Advanced Bus-Clamping PWM (ABCPWM) type-2. In these vector sequences, over a sub-cycle period, one phase is switched double and one phase is switched once and another phase remains clamped. Some times these vector sequences are known as "Double Switching PWM" sequences.

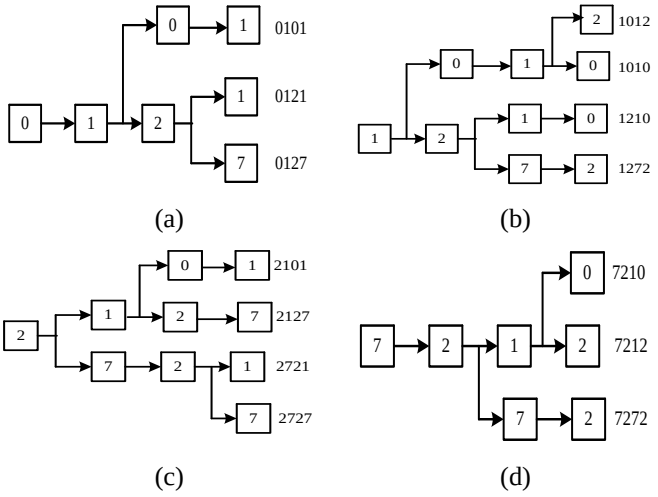

Fig.3: Different possible vector sequences starting with (a) vector-0, (b) vector-1, (c) vector-2 and (d) vector-7 for 2-level VSI in sector-1

To reduce the switching loss and current ripple, there exists another two sequences (012-210) and (721-127). These sequences are known as Bus-Clamping PWM (BCPWM). At high modulation index and same average switching frequency, line current ripple is lesser with BCPWM compare to CSVPWM. On the other hand, at high modulation index and same carrier frequency, the switching loss is lesser in case of BCPWM compare to CSVPWM. At high modulation index, ABCPWM is better than BCPWM like reduction in line current ripple. The hexagon for 30^0 BCPWM is shown in Fig. 2(b), for each quarter of fundamental cycle, one phase gets clamped either to positive DC link or negative DC link. The swapping of vector sequence in subsectors under a sector (like 721-127 is for first subsector in sector-1 and 012-210 is for second subsector in sector-1) gives 60^0BCPWM. In this PWM, each phase gets clamped middle 60^0 duration of each fundamental cycle. Fig. 2(c) and 2(d) show the hexagon for 30^0ABCPWM Type-1 and 30^0 ABCPWM Type-2 respectively. The swapping of vector sequence between subsectors in a sector give the 60^0ABCPWM. From the sequences it can observe that the number of switching for 012 is 2 where as for the other vector sequences the number of switching is three over a T_s. So for same average switching frequency over the fundamental cycle or line cycle, the sub-cycle period for 012 is 2/3 of that for other sequences. On the other hand, for 012, 0121 and 1012, a phase (here B-Phase) gets clamped, these vector sequences are also known as "Clamping Sequences or Discontinuous PWM sequences". It has been already proven that ABCPWM is better than BCPWM and CSVPWM at high modulation indices at same average switching frequency **[11-14]**.

International Journal of Engineering Research & Technology (IJERT)
ISSN: 2278-0181
Vol. 6 Issue 04, April-2017

Table-2: Different vector sequences for 2-level VSI

Name	Vector Sequence	Valid/ not-Valid	Reason
CSVPWM	0127-7210	Valid	conditions (1-4) are satisfied
Special PWM 1	0121-1210	Valid	conditions (1-4) are satisfied
Special PWM 1	7212-2127	Valid	conditions (1-4) are satisfied
Special PWM 2	1012-2101	Valid	conditions (1-4) are satisfied
Special PWM 2	2721-1272	Valid	conditions (1-4) are satisfied
xxxxxxxxx	0101-1010	not-Valid	condition 2 is not satisfied
xxxxxxxxx	7272-2727	not-Valid	condition 2 is not satisfied
Bus-Clamping PWM	012-210	Valid	conditions (1-4) are satisfied
Bus-Clamping PWM	721-127	Valid	conditions (1-4) are satisfied

IV. SHOOT THROUGH STATE FOR ZSI

In ZSI, the shoot-through state is generated in seven possible switching combinations which is listed in Table-3. ST_1, ST_2 and ST_3 are generated by simultaneously turning ON both switches of R-phase leg, Y-phase leg and B-phase leg of inverter respectively. These shoot-through states give minimum number of switching transition that means minimum switching loss. Each of these type of shoot-through has four kind of switching combination i.e. other two phases can switched in four combination. In the Table-3, X denotes either ON (1) or OFF (0).

Table-3: Shoot-through states for 2-level ZSI

ST-State	S_1	S_4	S_3	S_6	S_5	S_2	Sub-State	Switching
ST_1	1	1	X	X	X	X	4	Minimum
ST_2	X	X	1	1	X	X		
ST_3	X	X	X	X	1	1		
ST_4	1	1	1	1	X	X	2	Medium
ST_5	X	X	1	1	1	1		
ST_6	1	1	X	X	1	1		
ST_7	1	1	1	1	1	1	0	Maximum

Similarly, ST_4, ST_5 and ST_6 are generated by simultaneously turning ON of R-Y phases, Y-B phases and B-R phases respectively. These kind of shoot-through states involve more number of switching transitions i.e. switching loss is more as compare to ST_1, ST_2 and ST_3. But the highest switching loss is involved with the shoot-through state ST_7 as it is generated by turning ON simultaneously all the switches of three phase legs. It involves highest number of switching transitions. So, for minimum switching loss, ST_1, ST_2 and ST_3 are chosen as the desirable shoot-through states.

V. SPACE VECTOR PWM FOR ZSI

In section-3, the different Space Vector based PWM techniques for 2-level VSI have been discussed. All these PWM techniques can be applied to switch ZSI. In **[9],** the conventional space vector PWM technique for ZSI has been proposed. Few studies have been done for other PWM techniques. A PWM technique for ZSI is implemented considering the following three control strategies- Simple Boost Control (SBC), Maximum Boost Control (MBC) and Constant Boost Control (CBC).

Table-4: Different vector sequences for ZSI

Name	Vector Sequence
CSVPWM	$0 \leftrightarrow ST_1 \leftrightarrow 1 \leftrightarrow ST_2 \leftrightarrow 2 \leftrightarrow ST_3 \leftrightarrow 7$
Special PWM 2	$1 \leftrightarrow ST_1 \leftrightarrow 0 \leftrightarrow ST_1 \leftrightarrow 1 \leftrightarrow ST_2 \leftrightarrow 2$
Special PWM 2	$2 \leftrightarrow ST_3 \leftrightarrow 7 \leftrightarrow ST_3 \leftrightarrow 2 \leftrightarrow ST_2 \leftrightarrow 1$
Special PWM 1	$0 \leftrightarrow ST_1 \leftrightarrow 1 \leftrightarrow ST_2 \leftrightarrow 2 \leftrightarrow ST_2 \leftrightarrow 1$
Special PWM 1	$7 \leftrightarrow ST_3 \leftrightarrow 2 \leftrightarrow ST_2 \leftrightarrow 1 \leftrightarrow ST_2 \leftrightarrow 2$
Bus-Clamping PWM	$0 \leftrightarrow ST_1 \leftrightarrow 1 \leftrightarrow ST_2 \leftrightarrow 2$
Bus-Clamping PWM	$7 \leftrightarrow ST_3 \leftrightarrow 2 \leftrightarrow ST_2 \leftrightarrow 1$

MBC gives maximum boosting factor and less switching stress as the total zero vector state is replaced by shoot-through state. The space vector hexagon for ZSI is similar to VSI as shown in Fig.2(a). The difference between vector sequences for VSI and ZSI is only the present of shoot through state in ZSI vector sequence. By inserting proper shoot-through, based on the advanced PWM for VSI, new PWM sequences for ZSI can be produced. Table-4 presents the different possible vector sequences for ZSI. It can be observed that for minimize the switching losses, only ST_1, ST2 and ST3 shoot-through states have been used in the proposed vector sequences.The division of shoot-through time period should be equal in a T_s. Unlike MBC, in SBC some portion of the traditional zero vector is replaced by shoot-through state. The timing diagrams for different PWM techniques for ZSI under SBC are shown in Fig.4. Fig.4.(a) shows the timing diagram corresponding to CSVPWM. In similar fashion, Fig.4.(b) and 4(c) present the timing diagrams corresponding special PWM-2 and special PWM-1 respectively. The timing diagram corresponding BCPWM is shown in Fig.4 (d). The dark portion in the timing diagrams indicates the shoot-through state duration. As shown from the timing diagrams that the vector sequence is selected in such way that the total number of switching over T_s is less than or equal to 3. The dwell times for different vectors for ZSI are similar to VSI except the zero vector time duration is divided into two equal parts. One part is replaced by total shoot-through state period, T_{ST}. The shoot-through time duration is equally divided into different shoot-through states for getting symmetric voltage waveform over T_s. The dwell times for ZSI in sector-1 are presented in (2). T_m is total zero vector plus shoot-through vector time duration. T_0 is the time period corresponding zero vector in SBC.

$$T_1 = M\frac{Sin(60^\circ-\alpha)}{Sin60^\circ}T_s\,;\,T_2 = M\frac{Sin\alpha}{Sin60^\circ}T_s \quad (2)$$

$$;$$

$$T_m = T_s - T_1 - T_2\,;\;\; T_{ST} = \frac{T_m}{2}\,;\;\; T_0 = \frac{T_m}{2}$$

International Journal of Engineering Research & Technology (IJERT)
ISSN: 2278-0181
Vol. 6 Issue 04, April-2017

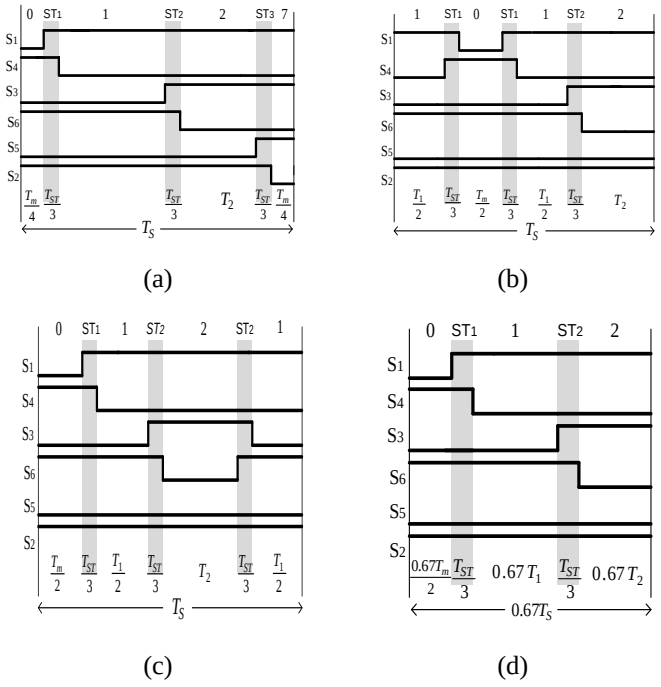

Fig.4: Timing diagrams of different PWM techniques for 2-level ZSI under SBC: Timing diagram corresponding to (a) CSVPWM (0127-7210), (b) Special PWM-2 (1012-2101) ,(c) Special PWM-1 (0121-1210) and (d)30^0 BCPWM (012-210)

VI. MAXIMUM BOOST CONTROL

In Maximum Boost Control (MBC), the total traditional zero vector duration is replaced by corresponding shoot-through state duration. As a result, the boosting factor increases and the voltage stress across switching device decreases. As the space vector hexagon is divided into equal six sector and symmetry to each other, the average shoot-through over fundamental cycle is same as that for one sector. The expression for average shoot-through duration ($\overline{T_{ST}}$), average shoot-through duty ratio ($\overline{D_0}$) and boosting factor, B under MBC are shown in (3).

$$\bar{T}_{ST} = \frac{3}{\pi}\int_0^{\frac{\pi}{3}} \left[T_s - \frac{2M}{\sqrt{3}} T_s \, Sin\left(\frac{\pi}{3}-\alpha\right) - \frac{2M}{\sqrt{3}} T_s \, Sin\alpha\right] d\alpha = \left[1 - \frac{2\sqrt{3}\,M}{\pi}\right] T_s$$

$$\bar{D}_0 = \frac{\bar{T}_{ST}}{T_s} = \left[1 - \frac{2\sqrt{3}M}{\pi}\right]; \; B = \frac{\pi}{4\sqrt{3}M - \pi} \qquad (3)$$

VII. CURRENT RIPPLE ANALYSIS BASED ON STATOR FLUX RIPPLE

The error voltage vector is defined as the difference between the applied voltage vector and desired reference vector. The error voltage vector corresponding applied vector $\vec{V}_1$, $\vec{V}_2$ and $\vec{V}_{0/7}$ are $\vec{V}_{e1}$, $\vec{V}_{e2}$ and $\vec{V}_{e0/7}$ respectively in sector-1 as shown in Fig-5. Table-5 presents the *d* and *q* components of error voltage vectors. The load or line current ripple of the inverter can be measured in term of stator flux ripple. The stator flux ripple vector is the time integral of error voltage vector. The measurement of stator flux ripple over a sub-carrier cycle is an adequate measurement of line/load current ripple over a sub-carrier cycle **[12-15]**. As in the previous section, the different vector sequences based on advanced PWM techniques for VSI, have been proposed for ZSI, the comparative study between them can be theoretically analyzed by the measurement of stator flux ripple over the sub-carrier cycle. In this section, the theoretical evaluation of RMS stator flux ripple over a sub-carrier cycle has been done for different vector sequences. As the number of switching for sequence 0-ST-1-ST-2 (ST stands for Shoot-Through) is less compare to other sequences as shown in the earlier section, the sub-carrier cycle for this sequence is considered as $0.67T_s$ but others remains same as T_s. But under maximum boost control technique, the zero vectors are replaced by corresponding shoot-through vectors. Under MBC, the number of switching (ON to OFF or OFF to ON) for ST-1-ST-2-ST and 1-ST-1-ST-2 are same and equal to 4. Whereas under MBC, the number of switching (ON to OFF or OFF to ON) for ST-1-ST-2-ST-1 and ST-1-ST-2 are 5 and 3 respectively. For evaluating the theoretical study under same average switching frequency, the sub-carrier cycle for ST-1-ST-2-ST, 1-ST-1-ST-2, ST-1-ST-2-ST-1 and ST-1-ST-2 are $0.8T_s$, $0.8T_s$, T_s and $0.6T_s$ respectively. For evaluating the time integral of error voltage vector, few quantities have been defined along the *q*-axis and *d*-axis. The quantities are the product of dwell times and the error voltage vector components along the *q* and *d* axes. The quantities are n_1, n_2 and n_Z corresponding to *q*-axis component of error voltage vector $\vec{V}_{e1}$, $\vec{V}_{e2}$ and $\vec{V}_{e0/7}$ respectively. $\vec{V}_{e0/7}$ does not have any component along the *d*-axis. The quantity along the *d*-axis for both $\vec{V}_{e1}$ and $\vec{V}_{e2}$ is denoted by A. The quantities are tabulated in the Table-6. The time integral of error voltage vector is drawn in *d*-*q* reference frame for a particular spatial angle, α . The stator flux ripple vector starts from origin and increasing in a particular direction same as the direction of corresponding error voltage vector. For example, for $\vec{V}_{e1}$, the stator flux ripple vector will increase in the direction of $\vec{V}_{e1}$ vector. The tip of stator voltage is forming a geometric shape in the reference frame and comes back to the origin again at the end of the sub-cycle period

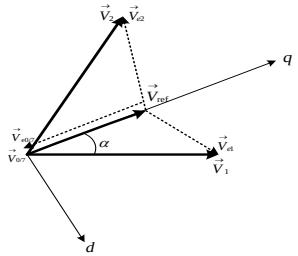

Fig.5: Error voltage vectors in sector-1

Table-5:Different error voltage vectors and corresponding *q* and *d* axis components in sector-1

Error Vector	Error Vector *q*-component	Error Vector *d*-component
$\vec{V}_{e1} = \vec{V}_1 - \vec{V}_{ref}$	$\vec{V}_{e1q} = \vec{V}_1 Cos\alpha - \vec{V}_{ref}$	$\vec{V}_{e1d} = \vec{V}_1 Sin\,\alpha$
$\vec{V}_{e2} = \vec{V}_2 - \vec{V}_{ref}$	$\vec{V}_{e2q} = \vec{V}_2 Cos(\frac{\pi}{3}-\alpha) - \vec{V}_{ref}$	$\vec{V}_{e2d} = -\vec{V}_2 Sin(\frac{\pi}{3}-\alpha)$
$\vec{V}_{ez} = \vec{V}_{0/7} - \vec{V}_{ref}$	$\vec{V}_{ezq} = -\vec{V}_{ref}$	0

International Journal of Engineering Research & Technology (IJERT)
ISSN: 2278-0181
Vol. 6 Issue 04, April-2017

Table-6: Different quantities when reference vector in sector-1

$(\text{Error Vector-Sec})_q$	$(\text{Error Vector-Sec})_d$
$n_1 = (V_1 \, Cos \ \alpha - V_{ref}) \bullet T_1$	$A = V_1 \, Sin \ \alpha \bullet T_1$
$n_2 = (V_2 \, Sin(\frac{\pi}{3} - \alpha) - V_{ref}) \bullet T_2$	$A = V_2 \, Sin \ (\frac{\pi}{3} - \alpha) \bullet T_2$
$n_z = V_{ref} \bullet T_{sh}$	0

The shape of the geometry is different for different vector sequences. The stator flux ripple vector can be decomposed into *d*-axis and *q*-axis components. Further, the components are drawn with respect to time. The variation of components of stator flux ripple vector with respect to time is different for different vector sequences as shown in Fig-6. The components consist of linear piece of lines and the slope of the line changes at the switching transition of vector sequence.

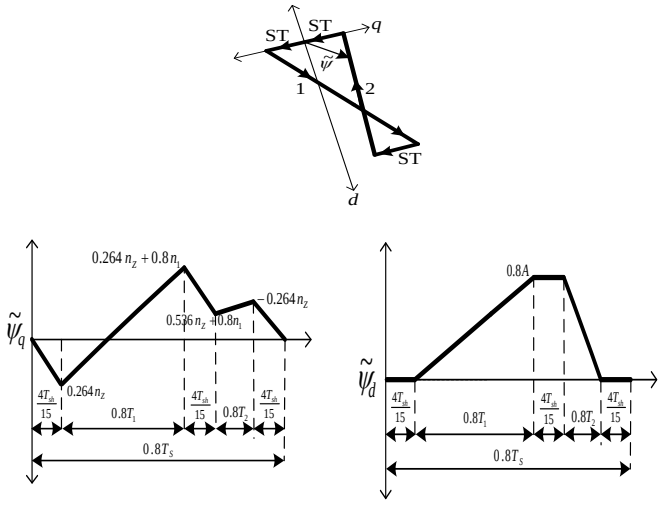

(a)

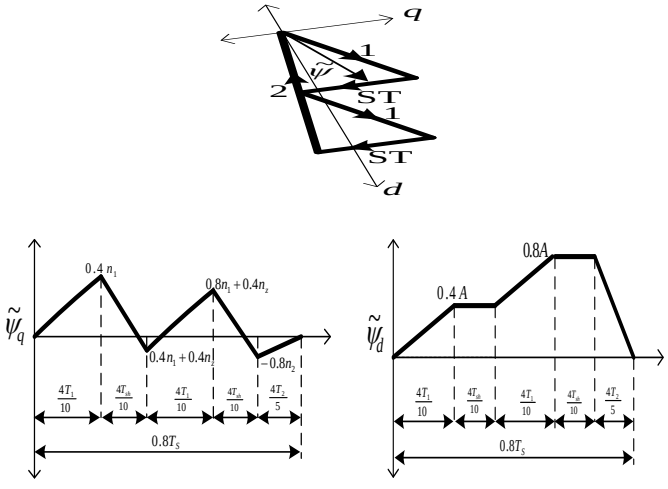

(b)

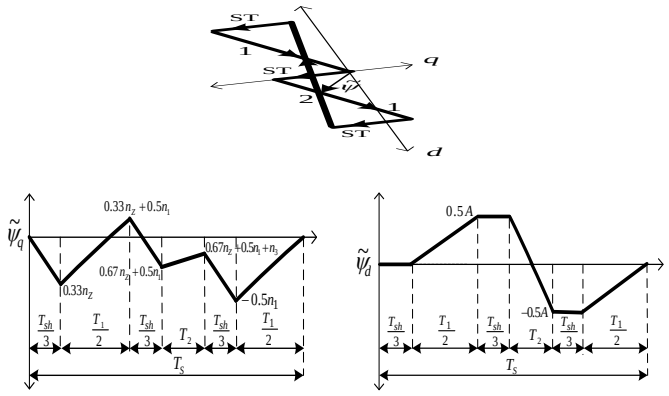

(c)

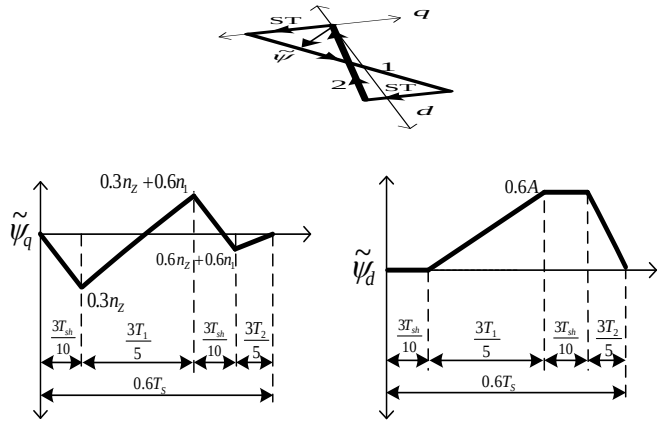

(d)

Fig-6: The variation of stator flux ripple in d-q reference frame over sub cycle and the variation of q and d axis components of stator flux ripple over one sub-cycle with time for (a) ST-1-ST-2-ST, (b) 1-ST-1-ST-2, (c) ST-1-ST-2-ST-1 and (d) ST-1-ST-2

For evaluating the RMS stator flux ripple over the sub-cycle, the RMS value of individual *d* and *q* axis need to be found. The square of linear piece of line becomes parabola. The RMS value of stator flux ripple is summation of individual *d* and *q* axis RMS value. RMS stator flux ripple- F_{0127}, F_{1012}, F_{0121} and F_{012}over a sub-cycle for ST-1-ST-2-ST, 1-ST-1-ST-2, ST-1-ST-2-ST-1 and ST-1-ST-2 respectively are expressed in square form in (4a), (4b), (4c) and 4(d) .

$$F_{0127}^2 = \frac{1}{3}(0.264n_z)^2 \frac{T_{sh}}{3T_s} +$$
$$\frac{1}{3}[(0.264n_z)^2 + (0.264n_z)(0.264n_z + 0.8n_1) + (0.264n_z + 0.8n_1)^2]\frac{T_1}{T_s} +$$
$$\frac{1}{3}[(0.264n_z + 0.8n_1)^2 + (0.264n_z + 0.8n_1)(0.536n_z + 0.8n_1) + (0.536n_z + 0.8n_1)^2]\frac{T_{sh}}{3T_s} +$$
$$\frac{1}{3}[(0.536n_z + 0.8n_1)^2 - (0.536n_z + 0.8n_1)(0.264n_z) + (-0.264n_z)^2]\frac{T_1}{T_s} + \quad 4(a)$$

International Journal of Engineering Research & Technology (IJERT)
ISSN: 2278-0181
Vol. 6 Issue 04, April-2017

$$\frac{1}{3}(-0.264n_z)^2\frac{T_{sh}}{3T_s}+\frac{1}{3}(0.8A)^2\left[\frac{T_1+T_{sh}+T_2}{T_s}\right]$$

$$F_{1012}^2=\frac{1}{3}(0.4n_1)^2\frac{T_1}{2T_s}+$$

$$\frac{1}{3}[(0.4n_1)^2+(0.4n_1)(0.4n_1+0.4n_z)+(0.4n_1+0.4n_z)^2]\frac{T_{sh}}{2T_s}+$$

$$\frac{1}{3}[(0.4n_1+0.4n_z)^2+(0.4n_1+0.4n_z)(0.8n_1+0.4n_z)+(0.8n_1+0.4n_z)^2]\frac{T_1}{2T_s}+$$

$$\frac{1}{3}[(0.8n_1+0.4n_z)^2-(0.8n_1+0.4n_z)(0.4n_z)+(-0.4n_z)^2]\frac{T_{sh}}{2T_s}+$$

$$\frac{1}{3}(-0.4n_z)^2\frac{T_{sh}}{T_s}+\frac{1}{3}(0.8A)^2\left[\frac{T_1}{T_s}+\frac{15T_{sh}}{8T_s}+\frac{T_2}{T_s}\right]$$

4(b)

$$F_{0121}^2=\frac{1}{3}(0.33n_z)^2\frac{T_{sh}}{3T_s}+$$

$$\frac{1}{3}[(0.33n_z)^2+(0.33n_z)(0.33n_z+0.5n_1)+(0.33n_z+0.5n_1)^2]\frac{T_1}{2T_s}+$$

$$\frac{1}{3}[(0.33n_z+0.5n_1)^2+(0.33n_z+0.5n_1)(0.67n_z+0.5n_1)+(0.67n_z+0.5n_1)^2]\frac{T_{sh}}{3T_s}+$$

$$\frac{1}{3}[(0.67n_z+0.5n_1)^2+(0.67n_z+0.5n_1)(0.67n_z+0.5n_1+n_2)+(0.67n_z+0.5n_1+n_2)^2]\frac{T_2}{T_s}+$$

$$\frac{1}{3}[(0.67n_z+0.5n_1+n_2)^2-(0.67n_z+0.5n_1+n_2)(0.5n_1)+(-0.5n_1)^2]\frac{T_{sh}}{3T_s}+$$

$$\frac{1}{3}(-0.5n_1)^2\frac{T_1}{2T_s}+\frac{1}{3}A^2\left[\frac{T_1}{4T_s}+\frac{T_{sh}}{2T_s}+\frac{T_2}{4T_s}\right]$$

4(c)

$$F_{012}^2=\frac{1}{3}(0.3n_z)^2\frac{T_{sh}}{2T_s}+$$

$$\frac{1}{3}[(0.3n_z)^2+(0.3n_z)(0.3n_z+0.6n_1)+(0.3n_z+0.6n_1)^2]\frac{T_1}{T_s}+$$

$$\frac{1}{3}[(0.3n_z+0.6n_1)^2+(0.3n_z+0.6n_1)(0.6n_z+0.6n_1)+(0.6n_z+0.6n_1)^2]\frac{T_{sh}}{2T_s}+$$

$$\frac{1}{3}[(0.8n_1+0.4n_z)^2-(0.8n_1+0.4n_z)(0.4n_z)+(-0.4n_z)^2]\frac{T_{sh}}{2T_s}+$$

$$\frac{1}{3}(0.6n_z+0.6n_1)^2\frac{T_{sh}}{T_s}+\frac{1}{3}(0.6A)^2\left[\frac{T_1}{T_s}+\frac{1.5T_{sh}}{T_s}+\frac{T_2}{T_s}\right]$$

4(d)

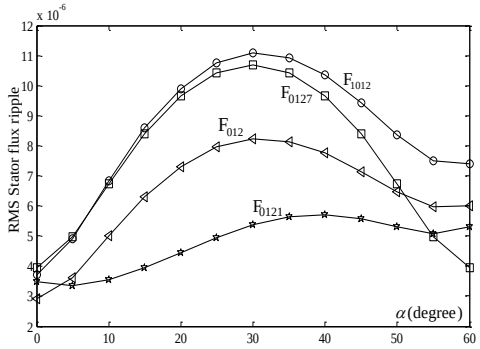

Fig-7: Variation of RMS stator flux ripple with α over a sector (V_{ref}=0.8 and T_s=1e^{-4} sec)

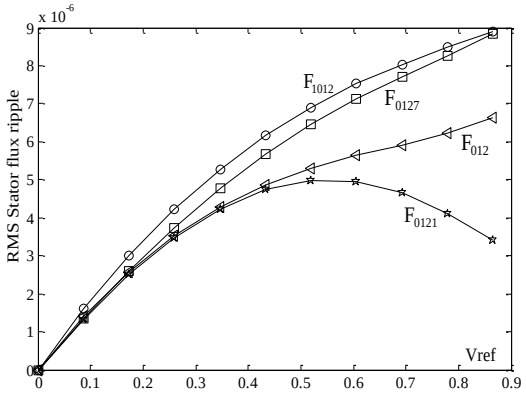

Fig-8: Variation of RMS stator flux ripple with reference vector V_{ref} (α =30^0 and T_s=1e^{-4} sec)

It can be observed from 4(a), 4(b), 4(c) and 4(d) that the RMS stator flux ripple depends on the spatial angle α, reference voltage magnitude, V_{ref} and sub-cycle period T_s. Fig-7 shows the variation of RMS stator flux ripple for different vector sequences for a spatial angle variation from 0^0 to 60^0 for V_{ref}=0.8 and T_s=1e-4 sec. It can be observed that RMS stator flux ripple is lowest for ST-1-ST-2-ST-1 (F_{0121}) in middle range of α. After that vector sequence ST-1-ST-2 gives the lesser RMS stator flux ripple compare to other sequences. Further the Fig-8 shows the variation of RMS stator flux ripple for a range of V_{ref} from 0 to maximum value 0.866 for spatial angle, α = 30^0 and sub-cycle period, T_s = 1e-4 sec. It can be observed that at higher value of V_{ref} (at higher modulation index), vector sequence ST-1-ST-2-ST-1 has lowest ripple compare to other vector sequences.

VIII. SIMULATION RESULTS

In this section, the simulation study of proposed PWM techniques have been done and verified with the theoretical analysis. For the simulation study, standard power electronics circuit simulator, Power-Sim software (PSim9.1.1) have been selected. All the PWM techniques have been implemented in this software with appropriate logical approach. On the other hand, for power circuit, the inductors and capacitors for Z-network have been selected according the specified current and voltage ripples. The simulation has been done considering R-L load and different motor load conditions.

International Journal of Engineering Research & Technology (IJERT)
ISSN: 2278-0181
Vol. 6 Issue 04, April-2017

A. Simulation study with 3-phase R-L load

With the following specifications, the simulation study for R-L load has been done-

1. Input DC voltage, Vin=162V
2. Load resistance R=100 Ω.
3. Load inductance, L=20mH
4. Switching frequency, f_{sw}=10kHz
5. Fundamental frequency, f_1=50Hz

The simulation study has been done considering variable modulation index and variable boosting factor condition.

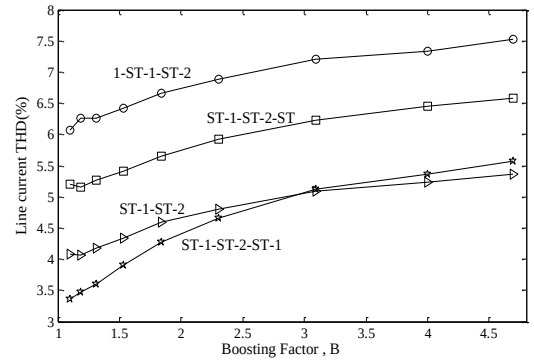

(a)

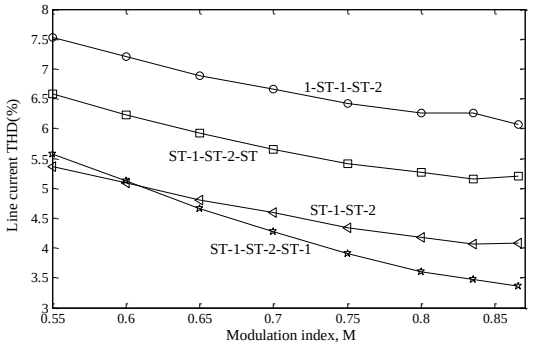

(b)

Fig-9: Variation of Simulated line current THD for different (a) boosting factor, (b) modulation index after applying different PWM vector sequence for R-L load (R=100 Ω , L=20mH)

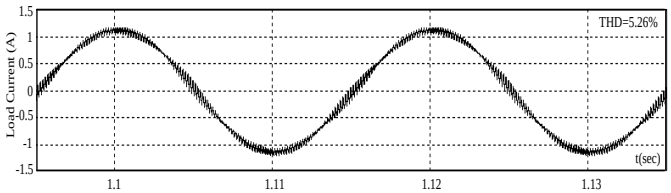

(a)

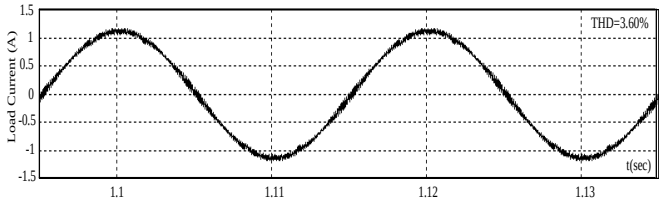

(b)

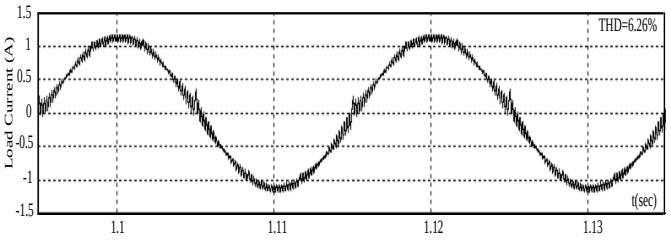

(c)

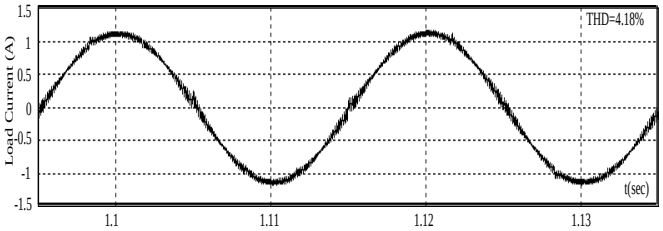

(d)

Fig.-10: Load current and its THD for R-L load for (a) ST-1-ST-2-ST, (b) ST-1-ST-2-ST-1, (c) 1-ST-1-ST-2 and (d)ST-1-ST-2 (modulation index=0.8)

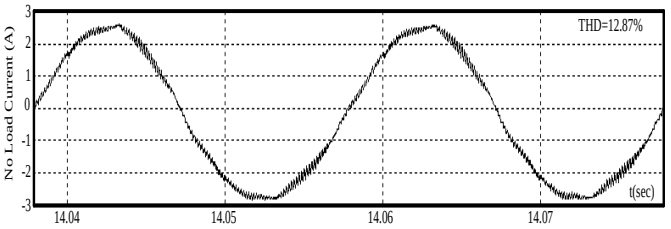

(a)

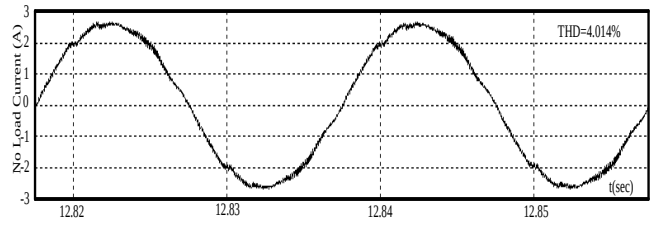

(b)

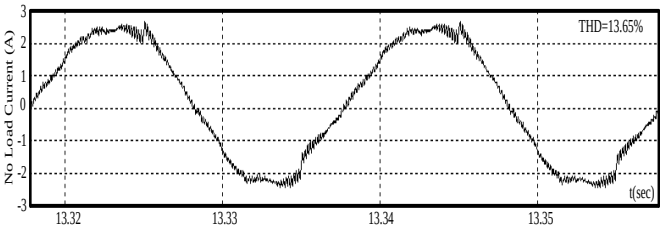

(c)

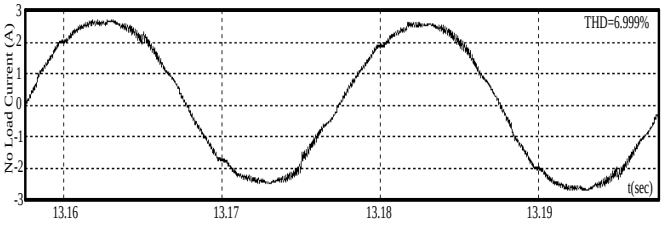

(d)

Fig.11: No Load Motor current and its THD for (a) ST-1-ST-2-ST, (b) ST-1-ST-2-ST-1, (c) 1-ST-1-ST-2 and (d)ST-1-ST-2 (modulation index=0.8)

International Journal of Engineering Research & Technology (IJERT)
ISSN: 2278-0181
Vol. 6 Issue 04, April-2017

The selection of the X-network inductors and capacitors by considering the following specifications-

1. Network is symmetric i.e. $L_1=L_2$ and $C_1=C_2$
2. Current ripple of the inductors is taken 5% of the input current.
3. Voltage ripple across the capacitors is 0.1% of capacitor voltage.

The calculated values of inductors and capacitors for Z-network are 18.466mH and 429μF.

Fig-9 presents the variations of line current THD for different values of modulation index and boosting factor for different PWM techniques with R=100Ω, L=20mH. It can be observed that ST-1-ST-2-ST-1 and ST-1-ST-2 vectors give the minimum THD compare to others two vector sequences. Further, at high modulation index, ST-1-ST-2-ST-1 is better than ST-1-ST-2 as shown in Fig.-9(b). Fig.-10 shows the line current waveforms for the specified R-L load conditions for different vector sequences. It is clearly observed that the quality of waveform is better for ST-1-ST-2-ST-1 compare to other vector sequences. Further, the measured THD of line current is lesser compare to that for other PWM techniques. After this, vector sequence ST-1-ST-2 gives lesser THD. Only vector sequence 1-ST-1-ST-2 gives higher THD compared to conventional space vector PWM sequence ST-1-ST-2-ST. This simulation study validates the theoretical study which has been presented in the previous section.

B. Simulation Study With 3-Phase Motor Load

A three phase Squirrel-Cage Induction motor with following specifications has been selected and simulated with ZSI under no-load, half full load and full load conditions under different PWM techniques. The specifications are-

1. Rated power=2HP
2. Rated RMS line to line voltage=208V
3. Stator resistance=4.2Ω
4. Rotor resistance=3Ω
5. Stator inductance=0.001H
6. Rotor inductance=0.001H
7. Magnetizing inductance=0.041H
8. Moment of inertia=0.7kg-m^2
9. No of pole=4
10. Operating frequency=50Hz

The simulation study has been done under modulation index 0.8. The calculated value of input voltage to the ZSI is 243.46V. It can be observed from Fig-11 that the vector sequence ST-1-ST-2-ST-1 gives the better quality of no load current waveform compare to other vector sequences. Under different load conditions, the THD values of load current for different sequences are tabulated in Table-7. It can be concluded that for any load conditions vector sequence ST-1-ST-2-ST-1 gives the lowest load current THD compare to others. After vector sequence ST-1-ST-2-ST-1, ST-1-ST-2 give the lowest load current THD. So, the theoretical analysis what has been done in the earlier sections is validated with the simulation study of motor load under different load conditions.

Table7: Load current THD under different load conditions under different PWM techniques

Load Condition	1-ST-1-ST-2	ST-1-ST-2-ST	ST-1-ST-2	ST-1-ST-2-ST-1
No Load	13.65%	12.87%	6.999%	4.014%
Half Load	11.8247%	11.484%	7.086%	3.8063%
Full Load	6.7897%	6.3142%	5.213%	3.9934%

IX. CONCLUSION

This paper proposes certain vector sequences based on advanced Space Vector based PWM techniques. By Psim simulation study of a ZSI, the effectiveness of the proposed techniques have been verified for R-L and different motor load conditions. The theoretical analysis and comparison of different sequences have been done by the concept of stator flux ripple which represents the line current ripple. The simulation study is validated with theoretical study. It has been observed that the propose sequences give lesser line current distortions and switching losses (as clamping is present) compare to classical SVPWM except 1-ST-1-ST-2 sequence. Further, same PWM techniques can be applied to other type of ZSI topologies like quasi-ZSI. Experimental validation of the proposed techniques can be future work. Further, hybrid PWM techniques for more reduction of output distortion for ZSI can be implement and verified in future. This study gives a new direction to the researcher in this area for implementing different real-time Space Vector based PWM techniques for different ZSIs.

REFERENCES

[1] F. Z. Peng, A. Joseph, J. Wang, M. Shen, L. Chen, Z.G. Pan, E.O. Rivera and Y. Huang, "Z-source inverter for motor drives," *IEEE Trans. Power Electron.*, vol. 20, no. 4, pp. 857-863, Jul. 2005.

[2] F. Z. Peng, M. Shen, and K. Holland, "Application of Z-source inverter for traction drive of fuel cell-battery hybrid electric vehicles," *IEEE Trans. Power Electron*, vol. 22, no. 3, pp. 1054-1061, May 2007.

[3] Y. Huang, M. Shen, F. Z. Peng and J. Wang, "Z-source inverter for residential photovoltaic systems," *IEEE Trans. Power Electron*, vol. 21, no. 6, pp. 1776-1782, Nov. 2006.

[4] Z. J. Zhou, X. Zhang, P. Xu, and W.X. Shen, " Single-phase uninterruptible power supply based on Z-source inverter," *IEEE Trans. Ind. Electron*, vol. 56, no.12, pp. 4894-4902, Dec. 2009.

[5] F. Z. Peng, "Z-source inverter," *IEEE Trans. Ind. Electron*, vol. 39, no.2, pp. 504-510, Mar./Apr. 2003.

[6] F. Z. Peng, M. S. Shen, and Z. Qian, "Maximum boost control of the Z-source inverter," *IEEE Trans. Power Electron*, vol. 20, no. 4, pp. 833-838, Jul. 2005.

[7] M.S. Shen, J. Wang, A. Joseph, F. Z. Peng, L. M. Tolbert and D.J. Adams, "Constant boost control of the Z-source inverter to minimize current ripple and voltage stress," *IEEE Trans. Ind. Appl.*, vol. 42, no. 3, pp. 770-777, May/Jun.. 2006.

[8] P.C. Loh, D. M. Vilathgamuwa, Y.S. Lai, G.T. Chua and Y.W. Li, "Pulse-width modulation of Z-source inverters," *IEEE Trans. Power Electron*, vol. 20, no. 6, pp. 1346-1355, Nov. 2006.

International Journal of Engineering Research & Technology (IJERT)
ISSN: 2278-0181
Vol. 6 Issue 04, April-2017

[9] Kun YU, Fang Lin LUO and Miao ZHU, "Space Vector Pulse-Width Modulation Base Maximum Boost Control of Z-Source Inverter," *IEEE International Symposium on Industrial Electronics (ISIE),* Hangzhou, pp. 521-526, 18th – 31th May, 2012.

[10] Sangeeta DebBarman and Tapas Roy, "Advanced pulse width modulation technique for Z-source inverter," *IEEE 6th India International Conference on Power Electronics (IICPE),* NIT Kurukshetra, India, pp. 1-6, 8th -10th Dec, 2014.

[11] G.Narayanan,H.K.Krishnamurthy,D. Zhao, and R.Ayyanar, "Advanced bus-clamping PWM techniques based on space vector approach," *IEEE Trans. Power Electron.*, vol. 21, no. 4, pp. 974–984, Jul. 2006.

[12] V.S.S.P.K. Hari and G. Narayanan, "Space-Vector-Based Hybrid Pulse Width Modulation Technique to Reduce Line Current Distortion in Induction Motor Drives," *IET Power Electronics,* Vol.-5, No-8, pp-1463-1471, Sept. 2012.

[13] A.R. Beig and V.T. Ranganathan," Space vector based bus clamped PWM algorithms for three level inverters: implementation, performance analysis and application considerations," *Applied Power Electronics Conference and Exposition,* Eighteenth Annual IEEE, vol. 1, pp: 569 – 575 , 2003.

[14] G. Narayanan, D. Zhao, H. K. Krishnamurthy, R. Ayyanar, and V. T. Ranganathan, "Space vector based hybrid PWM technique for reduced current ripple," *IEEE Trans. Ind. Electron.*, vol. 55, no. 4, pp. 1614– 1627,Apr.2008.